Quantum Fluctuations in Small Lasers

Kaushik Roy-Choudhury and Stephan Haas
Department of Physics and Astronomy, University of Southern California, Los Angeles, California 90089-0484, USA

A. F. J. Levi
Department of Physics and Astronomy, University of Southern California, Los Angeles, California 90089-0484, USA
Department of Electrical Engineering, University of Southern California, Los Angeles, California 90089-2533, USA

(Received 12 September 2008; published 5 February 2009)

The dominant role of quantum fluctuations in determining the steady-state and transient response of a laser is demonstrated when there is a small number of particles in the system. In this regime, quantum fluctuations are found to suppress the lasing threshold and create a non-Poisson probability distribution for n discrete excited electronic states and s discrete photons. The correlation between n and s damps the averaged dynamic response of laser emission. Random walk calculations verify the master equation predictions and are used to connect to systems containing larger numbers of particles.

DOI: 10.1103/PhysRevLett.102.053902 PACS numbers: 42.55.Ah, 42.55.Sa

The behavior of a conventional laser is relatively well understood in the thermodynamic limit. There is a large number of excited states in the system, the fraction of spontaneous emission, β, feeding into the lasing optical mode is small ($\beta \to 0$) and there is a well-defined lasing threshold that marks the transition between nonlasing and lasing light. These systems may be described in terms of a continuum mean-field approach using rate equations. More complete quantum statistical theories of laser operation in the large particle number limit reproduce the mean-field results. Such models include a description in terms of Fokker-Plank equations by Haken [1] and a density matrix approach by Scully and Lamb [2–4]. The ensemble averages used in these models cannot be applied to the small systems we consider.

A new paradigm arises for laser diode operation when there is only a small number of excited states in the system. In this work we show that *quantum fluctuations in small lasers suppress lasing and enhance spontaneous emission*. This remarkable observation is contrary to expectations of conventional Landau-Ginzburg theory of phase transitions in which fluctuations are expected to enhance lasing below threshold. This in turn raises the more general question of which alternative theoretical framework would be more appropriate to describe dynamical crossover processes in small quantum systems.

To capture the physics dominating the mesoscale behavior we use master equations that quantize particle number. Previously, such equations have been solved to explore steady-state behavior in the limit of cavity quantum electrodynamics for which $\beta = 1$ [5,6]. Here, we model the steady-state *and* transient response of scaled laser diodes in which the number of excited electronic states, n, and the number of photons, s, in the lasing mode of frequency ω are correlated such that $\langle ns \rangle$ may not be factorized to $\langle n \rangle \times \langle s \rangle$. In this situation there are significant differences in predicted behavior compared to continuum mean-field theory.

The equation describing time evolution of probability $P_{n,s}$ of states (n, s) in a single-mode semiconductor laser diode with active cavity volume V driven by current I is of the form

$$\frac{dP_{n,s}}{dt} = -\kappa(sP_{n,s} - (s+1)P_{n,s+1}) - (sG_nP_{n,s} - (s-1)G_{n+1}P_{n+1,s-1}) - (sAP_{n,s} - (s+1)AP_{n-1,s+1}) - \beta B(n^2P_{n,s} - (n+1)^2P_{n+1,s-1}) - (1-\beta)B(n^2P_{n,s} - (n+1)^2P_{n+1,s}) - \frac{I}{e}(P_{n,s} - P_{n-1,s}) \quad (1)$$

Figure 1 illustrates the transitions in and out of state (n, s). The term $-Bn^2P_{n,s}(t)$ denotes spontaneous emission of photons involving transitions from state (n, s) to state $(n-1, s+1)$ where $B = B'/V$ and B' is the spontaneous emission coefficient. $-sG_nP_{n,s}(t)$ describes stimulated emission of photons from state (n, s) to state $(n-1, s+1)$, where G_n is the stimulated emission coefficient. $-(1-\beta)Bn^2P_{n,s}(t)$ is the decay of electrons into nonlasing photons via transitions from state (n, s) to state $(n-1, s)$. $-IP_{n,s}(t)$ denotes pumping of electrons causing transitions from state (n, s) to state $(n+1, s)$. $-AsP_{n,s}(t)$ is stimulated absorption of photons involving transitions from state (n, s) to state $(n+1, s-1)$ where A is the stimulated absorption coefficient. $-\kappa sP_{n,s}(t)$ describes the decay of cavity photons in which transitions from state (n, s) to state $(n, s-1)$ occur, where κ is the optical loss coefficient.

The time evolution of $P_{n,s}$ can be solved by integrating (1). $P_{n,s}$ may also be solved under steady-state conditions by truncating the system at values of n and s which are

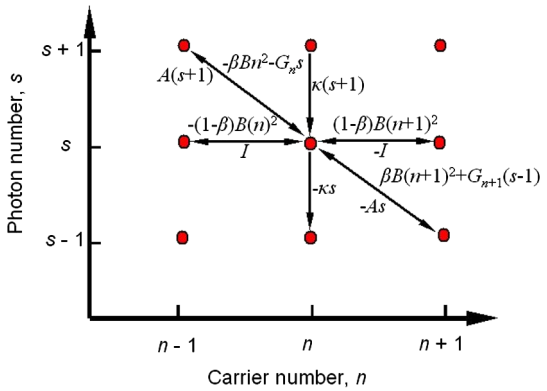

FIG. 1 (color online). Transition rates in and out of state (n, s). Positive signs indicate flow into the state and negative signs flow out of the state. $-G_n s = (a\Gamma cn/Vn_r)s$ is the stimulated emission rate in the system at photon energy $\hbar\omega$, $-As = (a\Gamma cn_0/Vn_r)s$ is the stimulated absorption rate, n_0 is the transparency carrier number, c is the speed of light in vacuum, Γ is the overlap of the optical field intensity with the gain medium, a is the gain slope coefficient, and n_r is the refractive index of the active volume V. The total optical loss rate from the Fabry-Perot cavity is $\kappa s = \frac{c}{n_r}(\alpha_i + \frac{1}{2L_c}\ln(\frac{1}{r_1 r_2}))s$, where $r_1 = r_2$ is the mirror reflectivity, α_i is the internal loss, and L_c is the cavity length. I is the injection (pump) current and e is the electron charge.

much larger than the steady-state mean values predicted by the continuum mean-field rate equations [5,6].

The continuum mean-field rate equations are derived from the master equations by averaging over all possible states after multiplying by n and s. This gives

$$\frac{d\langle n\rangle}{dt} = -B\langle n^2\rangle - \frac{a\Gamma c}{Vn_r}\langle(n - n_0)s\rangle + \frac{I}{e}, \qquad (2)$$

$$\frac{d\langle s\rangle}{dt} = \beta B\langle n^2\rangle + \frac{a\Gamma c}{Vn_r}\langle(n - n_0)s\rangle - \kappa\langle s\rangle, \qquad (3)$$

which reduces to the rate equations if $\langle(n - n_0)s\rangle = \langle(n - n_0)\rangle\langle s\rangle$. However, in a system involving a small number of particles this factorization approximation is not valid, leading to differences between the predictions of continuum mean-field theory and a more complete probabilistic picture.

Figure 2 illustrates some of the essential differences by calculating the steady-state characteristics with master equations (M.E.) and continuum mean-field rate equations (R.E.). The $\langle ns\rangle$ correlation near threshold which is present in the master equation calculation increases the apparent threshold current to a value greater than that predicted by the rate equations [Fig. 2(a)], causes depinning of carriers, and a peak in the mean electron number $\langle n\rangle$ [Fig. 2(b)].

Fluctuations in photon number may be quantified using the Fano factor

$$F = \sigma_s^2/\langle s\rangle, \qquad (4)$$

where σ_s is the standard deviation in photon number. For a conventional laser this quantity peaks sharply at the lasing threshold current I_{th}. For large injection currents, $I \gg I_{\text{th}}$, the Fano factor approaches unity, corresponding to a Poisson distribution. For small cavities a broad peak in the Fano factor occurs in the vicinity of the threshold, and $F > 1$, indicating a non-Poisson distribution. Assuming the value of current at the Fano-factor peak may be used as a measure of laser threshold; Fig. 2(c) gives a threshold $I_{\text{th}} = 45$ nA which is considerably greater than the value of $I_{\text{th}} = 10$ nA predicted by continuum mean-field rate equations. Figure 2(d) shows that the electron-photon correlation $\langle ns\rangle$ differs the most from the product of means $\langle n\rangle\langle s\rangle$ near the

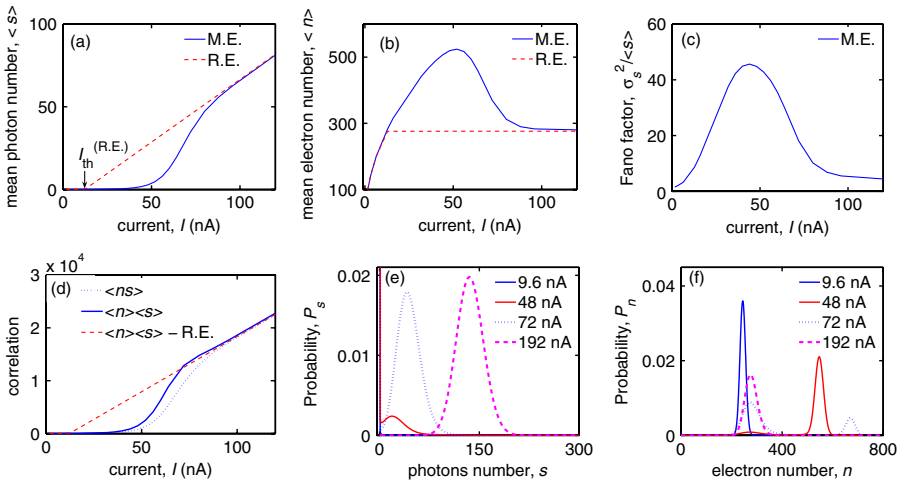

FIG. 2 (color online). Steady-state characteristics. (a) Calculated mean photon number as a function of current showing that M.E. predict suppression of lasing threshold relative to mean-field R.E. calculations. Suppression in lasing is due to quantum fluctuations. (b) Calculated mean electron number as a function of current. M.E. show carrier depinning due to quantum fluctuations. (c) Fano-factor $F = \sigma_s^2/\langle s\rangle$ as a function of current, I. (d) Electron-photon correlation and product of means versus current. (e) Probability of photons for different currents. (f) Probability of electrons for different currents. Parameters: $V = (0.1\ \mu\text{m} \times 0.1\ \mu\text{m} \times 10\ \text{nm})$, $\Gamma = 0.25$, $a = 2.5 \times 10^{-18}\ \text{cm}^2\,\text{s}^{-1}$, $B' = 10^{-10}\ \text{cm}^3\,\text{s}^{-1}$, $n_0 = 10^{18}\ \text{cm}^{-3}$, $\alpha_i = 1\ \text{cm}^{-1}$, $n_r = 4$, $r = 1\text{–}10^{-6}$, $\beta = 10^{-4}$.

threshold region. This behavior however disappears as we scale to larger number of particles, approaching the limit of conventional laser operation.

Figures 2(e) and 2(f) show the probability distribution of electrons P_n and photons P_s for different stages of laser operation. At low injection currents P_s is bimodal with a large probability for $s = 0$, which indicates that quantum fluctuations cause lasing emission to turn off. The probability distribution for P_s and P_n near I_{th} is bimodal. Only when $I \gg I_{\mathrm{th}}$ do P_s and P_n become single peaked.

The peak in mean electron number near threshold shown in Fig. 2(b) may be studied in more detail by modifying the master equations to include spontaneous emission of photons into a nonlasing channel. The $(1 - \beta)$ term in (1) feeds into another channel containing s' photons which decay at the same rate as the cavity photons. This channel does not participate in any stimulated processes and so avoids the correlation effects that strongly influence lasing emission. The master equation for probability $P_{n,s,s'}(t)$ is (1) with additional terms $(1 - \beta)Bn^2P_{n,s,s'}$ corresponding to decay of electrons into photons of the nonlasing channel, causing a transition from state (n, s, s') to $(n - 1, s, s' + 1)$ and $\kappa s' P_{n,s,s'}$ denoting decay of nonlasing photons, causing a transition from state (n, s, s') to $(n, s, s' - 1)$. The average value for n and s obtained using $P_{n,s,s'}(t)$ gives Eqs. (2) and (3) respectively. The average for s' is

$$\frac{d\langle s'\rangle}{dt} = (1 - \beta)B\langle n^2\rangle - \kappa\langle s'\rangle. \tag{5}$$

Thus the nonlasing spontaneous emission channel will peak with the mean number of carriers near threshold as lasing is suppressed, and will eventually be pinned along with the carriers for higher values of current. From this one may conclude that in small cavities the correlation of electrons and lasing photons suppresses lasing across threshold and results in enhanced spontaneous emission.

Figures 3(a) and 3(b) show the time evolution of $\langle n\rangle$ and $\langle s\rangle$ for a small laser operating above threshold. Factorization of the correlation $\langle ns\rangle$ is not possible, and the continuum mean-field rate equation results do not converge to the master equation solution. Figures 3(c) and 3(d) show that at any point in time the instantaneous probability $P_{n,s}$ carries information about the path taken. In contrast, averaging in the mean-field calculation removes information about the system's history.

The response to a step change in current indicates a slowing of the system on average in regimes where correlation effects dominate. An increase in the cavity size, while keeping other parameters fixed, yields a smaller difference compared to mean-field predictions and convergence is achieved for both static and dynamic characteristics for larger cavity sizes.

The cavity parameters used for the results shown in Fig. 2 and 3 were idealized for computational convenience. However, the underlying physics, in which quantum fluctuations suppress lasing and carriers are depinned, remains

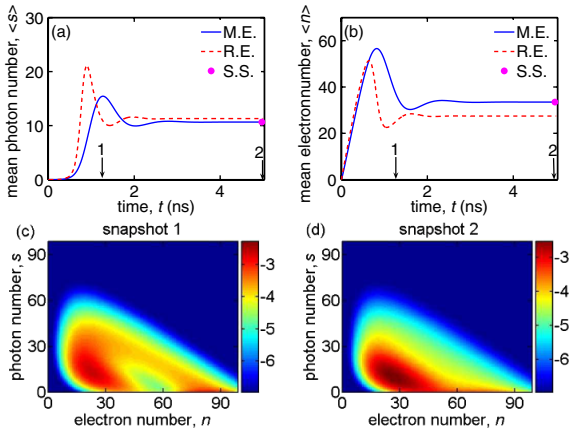

FIG. 3 (color online). Transient behavior of mean electron number and photon number for a step change in current from $I(t < 0) = 0$ to $I(t \geq 0) = 100$ electron/ns ($= 16$ nA). (a) Mean photon number vs time. (b) Mean electron number vs time. The dot at the last time point denotes the mean calculated from the probability distribution obtained by the steady-state technique. (c) $P_{n,s}$ calculated at time $t = 1.25$ ns and indicated by arrow labeled 1 in (a) and (b). (d) $P_{n,s}$ calculated at time $t = 5$ ns and indicated by arrow labeled 2 in (a) and (b). Parameters as in Fig. 2 but with $V = (0.1\ \mu\mathrm{m} \times 10\ \mathrm{nm} \times 10\ \mathrm{nm})$ and $\beta = 10^{-1}$.

valid. Use of realistic parameters increases the number of particles leading to a computationally cumbersome number of probability states. To connect with realistic parameters and systems containing larger numbers of particles we use a random walk calculation. This not only reproduces the master equations result but also makes similar predictions for small systems with experimentally accessible parameters.

Consider the system at time $t = 0$ containing n excited electronic states and s photons. It can undergo any of the allowed processes to move to a neighboring point on the grid described by Fig. 1. When the system resides in state (n, s), the time constants, τ_i, of all possible independent transition channels are calculated. The next time step is calculated using $t_i = -\tau_i \ln(\mathcal{R})$ where the subscript labels the channel and $\mathcal{R}$ is a uniformly distributed random number between zero and one. The channel with the lowest t_i is chosen and the system makes a move to the new state in time t_i. When averaged over large data sets, the random walk method converges to the master equation results. The process is a biased random walk on a grid whose trajectories sample the solution of the master equation.

To obtain steady-state probability distributions of electrons and photons at a particular current, averages over 100 trajectories are computed, with each trajectory consisting of 2×10^6 time steps. The probability distributions are computed from the relative time spent in each state (n, s).

Figure 4 shows trajectories in the time-domain for different injection currents. The probability distribution for these injection currents obtained from the master equations are shown in Figs. 2(e) and 2(f). In the long-time limit, trajectories in the (n, s) plane converge to the predictions of

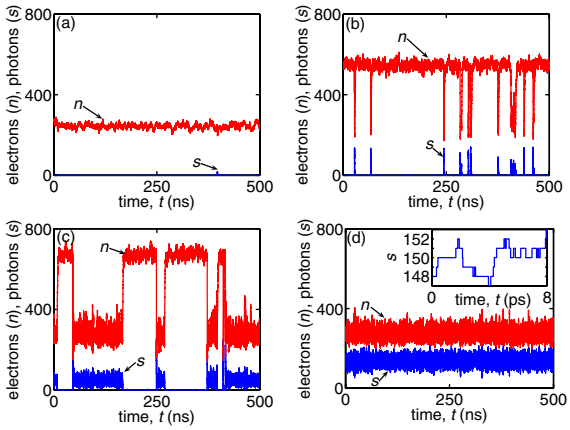

FIG. 4 (color online). Time evolution of electrons and photons calculated by the random walk method. (a) Current, $I = 9.6$ nA. (b) $I = 48$ nA. (c) $I = 72$ nA. (d) $I = 192$ nA. The inset shows discrete step changes in photon number with time. Parameters as in Fig. 2.

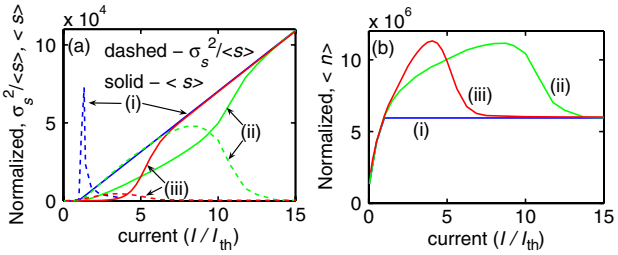

FIG. 5 (color online). Comparison of steady-state laser characteristics for 3 cavities. (a) Normalized mean photon number and Fano factor versus current. (b) Normalized mean electron number versus current. (i) Represents a large cavity, (ii) represents an intermediate cavity, (iii) represents a small cavity (Fig. 2). The large cavity matches the rate equation data closely. The rate equation data for the other two cases are multiplied by constant factors (normalization constants) to overlap the large cavity data. The current values are divided by the respective threshold currents predicted by rate equations ($I_{\text{th-i}} = 112$ μA, $I_{\text{th-ii}} = 320$ nA, $I_{\text{th-iii}} = 12.8$ nA). Normalization constants, N are Mean photon number, $N(s)_{\text{i}} = 1$, $N(s)_{\text{ii}} = 350$, $N(s)_{\text{iii}} = 800$. Mean electron number, $N(n)_{\text{i}} = 1$, $N(n)_{\text{ii}} = 607$, $N(n)_{\text{iii}} = 21\,594$. Fano factor, $N(F)_{\text{i}} = 10$, $N(F)_{\text{ii}} = 10$, $N(F)_{\text{iii}} = 100$. Parameters: $V_{\text{i}} = (5\ \mu\text{m} \times 1\ \mu\text{m} \times 1\ \mu\text{m})$, $V_{\text{ii}} = (5\ \mu\text{m} \times 0.1\ \mu\text{m} \times 10\ \text{nm})$, $V_{\text{iii}} = (0.1\ \mu\text{m} \times 0.1\ \mu\text{m} \times 10\ \text{nm})$, $\Gamma_{\text{i,iii}} = 0.25$, $\Gamma_{\text{ii}} = 0.05$, $a_{\text{i,ii}} = 2.5 \times 10^{-16}\ \text{cm}^2\,\text{s}^{-1}$, $a_{\text{iii}} = 2.5 \times 10^{-18}\ \text{cm}^2\,\text{s}^{-1}$, $B' = 10^{-10}\ \text{cm}^3\,\text{s}^{-1}$, $n_0 = 10^{18}\ \text{cm}^{-3}$, $\alpha_i = 10\ \text{cm}^{-1}$ for (i),(ii), $\alpha_i = 1\ \text{cm}^{-1}$ for (iii), $n_r = 4$, $r_{\text{i,ii}} = 0.999$, $r_{\text{iii}} = 1\text{–}10^{-6}$ and $\beta = 10^{-4}$.

the master equations [Fig. 3(d)]. The time-domain data in Figs. 4(a) and 4(b) shows bursts of photons because the injection current is not great enough to sustain continuous lasing. Figure 4(c) demonstrates that at higher injection current longer photon bursts result in a double-peaked average electron distribution. Figure 4(d) shows strong lasing with quantized fluctuations in photon number about a mean value $\langle s \rangle = 150$.

In Fig. 5, we compare the steady-state laser characteristics of (i) a large active volume cavity ($V = 5\ \mu\text{m}^3$), (ii) an intermediate size ($V = 5 \times 10^{-3}\ \mu\text{m}^3$), and (iii) a small size ($V = 10^{-4}\ \mu\text{m}^3$). The data are normalized to the large active volume cavity rate equation predictions for $\langle n \rangle$ and $\langle s \rangle$. Figure 5(a) shows that the calculation of $\langle s \rangle$ as a function of I converges to the continuum mean-field rate equation result for the largest size, and that lasing is increasingly suppressed as the active volume is decreased. The corresponding normalized Fano-factor peaks in Fig. 5(a) illustrate the presence of strong fluctuations and non-Poisson photon statistics. Figure 5(b) shows the depinning of the average electron number in the region where photon fluctuations are strongest. Time-domain data illustrated in Fig. 4(c) demonstrates that the system fails to lase continuously in this region. As the electron number in the cavity increases with increasing cavity size, more spontaneous emission events become possible. Spontaneous emission in a cavity with no photons initiates the first stimulated processes. So a large number of such events enables the system to lase continuously. A lesser likelihood of such events in a small active volume laser causes suppression of continuous lasing. If the system loses all its photons, it has to wait for the next spontaneous emission event.

In conclusion, the steady-state and transient response of a laser is driven by quantum fluctuations when there are a small number of particles in the system. These fluctuations, and the fact that a lowest energy state of the system exists, suppress lasing and enhance spontaneous emission around threshold. Dynamic switching between two system states dominates the fluctuations. Correlations between n discrete excited electronic states and s discrete photons create a non-Poisson probability distribution and damp the average dynamic response of laser emission.

We acknowledge support by the Department of Energy under grant DE-FG02-05ER46240 and the National Science Foundation grant ECCS-0507270.

[1] H. Haken, *Handbuch der Physik*, edited by L. Genzel (Springer, Berlin, 1970), Vol. XXV/2c.
[2] M. O. Scully and W. E. Lamb, Phys. Rev. Lett. **16**, 853 (1966).
[3] M. O. Scully and W. E. Lamb, Phys. Rev. **159**, 208 (1967).
[4] M. O. Scully and M. Suhail Zubairy, *Quantum Optics* (Cambridge University Press, Cambridge, England, 1997).
[5] Perry R. Rice and H. J. Carmichael, Phys. Rev. A **50**, 4318 (1994).
[6] H. J. Carmichael, *Proceedings of the International School on Lasers and Quantum Optics, Mar del Plata, Argentina, 22-31 August, 1988* (World Scientific, Singapore, 1990), p. 52.